communications earth & environment

ARTICLE

https://doi.org/10.1038/s43247-022-00562-y OPEN

Opposing comparable large effects of fine aerosols and coarse sea spray on marine warm clouds

Fan Liu[1], Feiyue Mao[1,2], Daniel Rosenfeld[2,3], Zengxin Pan[2,3]✉, Lin Zang[4], Yannian Zhu[5,6], Jianhua Yin[1] & Wei Gong[2,4]

Fine aerosols, by acting as cloud condensation nuclei, suppress rainfall and enhance the albedo and coverage of marine warm clouds, thereby partly counteracting the greenhouse-induced warming. While this is relatively well documented, the co-existing opposite effects of giant cloud condensation nuclei from coarse sea spray aerosols are poorly quantified. Here, satellite measurements show that the effects of coarse sea spray aerosols have comparable magnitudes with opposite sign to those of fine aerosols. For fixed cloud liquid water path and coarse sea spray aerosols, increasing fine aerosols decreased rainfall flux and cloud drop effective radius by a factor of 1/4 and 40%, respectively. Conversely, for fixed fine aerosols and cloud liquid water path, added coarse sea spray aerosols enhanced rainfall flux and cloud drop effective radius by a factor of 4 and 35%, respectively. These large and contrasting effects are independent on meteorological conditions. These processes must be fully incorporated into climate models to faithfully represent aerosol effects on clouds, precipitation, and radiative forcing.

[1] School of Remote Sensing and Information Engineering, Wuhan University, 430079 Wuhan, China. [2] State Key Laboratory of Information Engineering in Surveying, Mapping, and Remote Sensing, Wuhan University, 430079 Wuhan, China. [3] Institute of Earth Sciences, The Hebrew University of Jerusalem, Jerusalem 91904, Israel. [4] School of Electronic Information, Wuhan University, 430079 Wuhan, China. [5] School of Atmospheric Sciences, Nanjing University, 210023 Nanjing, China. [6] Joint International Research Laboratory of Atmospheric and Earth System Sciences & Institute for Climate and Global Change Research, Nanjing University, 210023 Nanjing, China. ✉email: pzx@whu.edu.cn

Warm clouds generally cover one-third of the global oceans and are crucial to Earth's radiation balance[1,2]. Aerosols are the most important factors for regulating warm cloud microphysics and coverage by serving as cloud condensation nuclei (CCN)[3]. A higher number of CCN produces more numerous and smaller cloud drops (Twomey effect)[4], suppresses warm rain by decreasing the collision–coalescence efficiency, increases cloud cover (cloud lifetime effect)[5,6], possibly enhances the cloud-top evaporation and dry air entrainment[7], and eventually affects the precipitation and Earth's radiative balance[3,8]. However, much uncertainty remains about the CCN effects on warm clouds. Previous studies found a decrease in rainfall rate from warm clouds[9,10] with added aerosols by acting as CCN, while other studies showed warm rainfall enhancements due to the aerosol convective invigoration effect[11]. Aerosols can also delay the time of rainfall onset[12], increase the height of rain initiation[13,14], or reduce the rainfall area of warm clouds[9].

In contrast, added giant CCN (GCCN) lower cloud base supersaturation and deactivate parts of the small CCN spectrum, reducing cloud drop concentrations and enhancing warm rain[15,16]. The GCCN can also accelerate warm rain initiation by larger initial cloud drop size[17–20]. Numerous model studies supported that GCCN enhance warm rain production albeit with inconsistent magnitudes[18,21,22]. However, other model studies have shown that GCCN have a very small or even negligible impact on warm rain initiation[12,23]. Observational studies for GCCN are very limited due to the difficulties in GCCN measurement, and they tend to support the GCCN enhancement of warm rain[21,24,25]. The above review shows that the effect of giant CCN (GCCN) from sea spray is still poorly quantified because it is difficult to measure and always co-exists with fine aerosols. This situation probably led to an underestimation of the effects of fine aerosols as well, although both physical processes are relatively well documented.

Additionally, cloud properties are determined by both meteorology and aerosols, and therefore must be disentangled[26–28]. Yang et al.[29] found that the wind speed is a major driver of the aerosol-cloud relationship over the mid-latitude oceans, because increasing wind speed enhances the emission of sea salt, evaporation rate, and transportation of water vapor into clouds. Chen et al.[8] observed a positive correlation between liquid water path (LWP) and aerosols under moist and stable conditions, while changing to a negative correlation when environmental conditions are dry and unstable due to the aerosol-enhanced entrainment. Rosenfeld et al.[3] found that when meteorological conditions are fixed, CCN can explain almost three-fourths of the variation in the radiative cooling effect of clouds, which is much stronger than in previous studies without the isolation of meteorological effect. This is supported by natural experiments such as volcanoes, industrial plumes and ship tracks[28], where similarly large indicated aerosol effects were accompanied by minimal meteorological variability. The meteorological co-variability with aerosols presents great challenges in evaluating and quantifying the aerosol effect on warm clouds and precipitation.

To address the questions above, as far as we know, we provide the first quantification of the combined effects of fine aerosols as CCN and coarse sea salt aerosols (CSA) as GCCN on cloud microstructure and warm rain after isolating the influence of meteorological factors. The focus of this research is on the oceans within the coverage of the METEOSAT Second Generation geostationary satellite from 50° W to 50° E and 30° S to 30° N and covers March 2014 to December 2017. The rainfall was obtained from the dual-frequency radar (DPR) onboard the Global Precipitation Mission satellite (GPM). Aerosols were obtained from the MERRA-2 reanalysis data. Please see more details in the "Methods section".

Results

Aerosol-driven warm rain variations at a fixed liquid water path. In general, warm rainfall over ocean is much more frequent than over land[30]. Previous studies indicate the differences in thermodynamic conditions (e.g. Bowen ratios[31], updraft[32,33]) play a critical role in the land-ocean warm rain contrast. For example, the lower updraft over ocean than over land allows more time for droplets' coalescence process, and may therefore promote the formation of warm rain. However, even with a similar meteorology[31,32], the much more frequent occurrence of warm rain over ocean than over land still exists. Here, we hypothesize that the abundant oceanic warm rain may be greatly contributed by the unique nature of fine aerosols and coarse sea salt aerosols over ocean.

Aerosols affect rainfall by influencing cloud properties[34]. As shown in Fig. 1a, larger cloud drop effective radius (r_e) and LWP produce a larger rainfall flux. This trend means that r_e and LWP control the rainfall with highly positive correlations. Since the atmospheric vertical thermodynamic profile determines cloud base height, temperature, and vertical development, the LWP captures much of the meteorological variability[3]. Thus, fixing LWP can help to separate the combined effects of meteorological

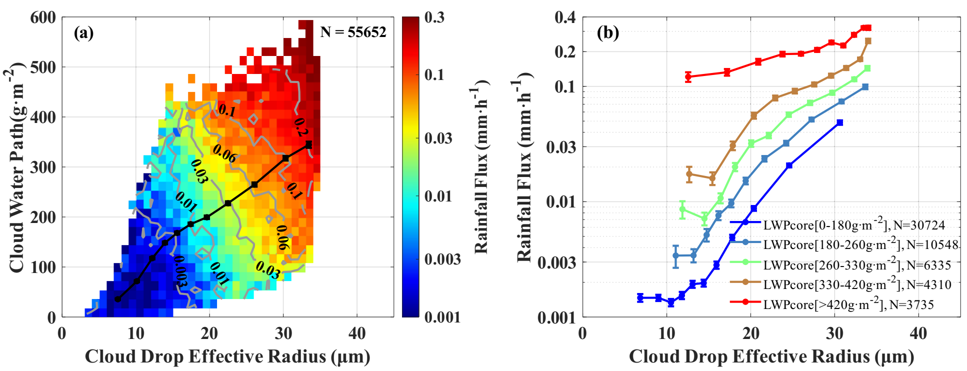

Fig. 1 Combined effects of cloud drop effective radius (r_e) and cloud liquid water path (LWP) on the rainfall flux. a The rainfall flux (including both rainfall and non-rainfall cases) from GPM DPR is a function of MSG CLAAS r_e and LWP. The color indicates the average rainfall flux. The minimum sample size for each bin is 10. The gray lines represent the contours of the rainfall flux that are indicated as different colors. The black line connects the dots, which are the averaged LWP at eleven bins of r_e, including the 0–5%, 5–15%, 15–25%, 25–35%, 35–45%, 45–55%, 55–65%, 65–75%, 75–85%, 85–95% and 95–100% quantiles. **b** The rainfall flux (averaging both rainfall and non-rainfall cases) changes with r_e at constant LWP bins. Vertical error bars indicate the standard error calculated by the standard deviation divided by the square root of the sample size.

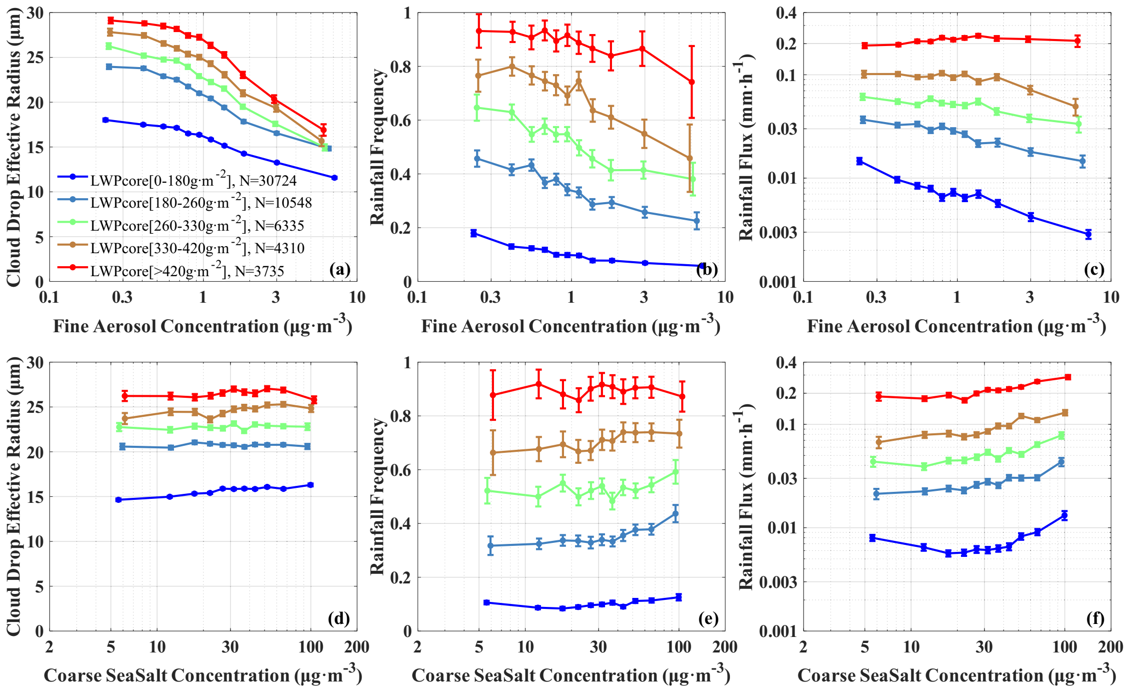

Fig. 2 Aerosol-driven cloud drop effective radius (r_e) and rainfall variations for fine aerosol (top) and coarse sea spray aerosols (CSA) (bottom) concentrations at constant cloud liquid water path (LWP) bins. Shown are **a** r_e, **b** rainfall frequency, and **c** flux variations (including both rainfall and non-rainfall cases) driven by fine aerosols. The **d–f** are the same as **a–c**, but for CSA. The color lines connect the dots, which are the averaged r_e, rainfall frequency and flux at eleven bins of fine (**a–c**) and CSA (**d–f**) aerosol concentrations, respectively, including the 0–5%, 5–15%, 15–25%, 25–35%, 35–45%, 45–55%, 55–65%, 65–75%, 75–85%, 85–95%, and 95–100% quantiles. Vertical error bars indicate the standard error.

factors. At a fixed LWP bin, the rainfall flux increases by an average factor of 20 with r_e increasing from 10 to 30 μm (Fig. 1b).

The responses of warm rain to aerosols differ with aerosol types, such as CCN and GCCN[21,35]. Figure S1a shows that the overall negative relationship of fine aerosol with warm rainfall is weak, while CSA is associated weakly positively with rainfall flux (Fig. S1b). Aerosol optical depth (Fig. S1c) is also weakly correlated with rainfall flux, as it is poorly related to CCN due to the co-variation with meteorology and observation limitation[36]. Pan et al.[16,37] showed that fine aerosol from MERRA-2 can be considered as a good proxy of CCN, and it can strongly enhance the convective mixed-phase rainfall, especially over land. It implies that the rain suppression by fine aerosols should be stronger than indicated in Fig. S1a. The contradiction of weak effects of fine aerosols on warm rain over ocean is hypothesized to be attributed to the offsetting effect of CSA.

We divided the data into different LWP bins and checked how fine aerosol and CSA could affect warm rainfall (Fig. 2). The lowest and highest bins indicate the 0–5% and 95–100% quantiles of aerosol concentration under the fixed LWP condition, and subsequent lowest and highest bins are defined similarly. The findings show that r_e largely decreases with added fine aerosols. The average reduction of r_e is 9.3 ± 1.6 μm (mean ± standard deviation) when fine aerosols increase from lowest to highest bins, with a maximum reduction of 12.2 μm occurring at the LWP bin of above 420 g m^{-2}. After fixing LWP, fine aerosol inhibits the rainfall frequency with an average reduction of 0.18 ± 0.10 and suppresses the rainfall flux by a factor of 0.56 ± 0.32. This suppression effect becomes weaker under higher LWP. In contrast, the effect of CSA was a slight increase in r_e and rainfall. Fine aerosols have a positive correlation with CSA, as shown in Fig. S2. Therefore, the contrasting effects of fine aerosol and CSA aerosols partially offset each other's influence, resulting in an apparent weak observed sensitivities of warm rainfall to aerosols. To separate the effects, we next analyze the effects of fine aerosols for fixed CSA and vice versa.

Isolate effects of fine aerosol and CSA on warm rainfall. Considering the co-variation between different types of aerosols, we quantified the effects of fine aerosol and CSA after fixing the other aerosol type, respectively. The average reduction of r_e with the increasing fine aerosol is 11.4 ± 0.9 μm (Fig. 3a), which is larger than the general result (9.3 ± 1.6 μm) mixed with CSA (Fig. 2a). Similarly, the suppression effect of fine aerosol was evident in the rainfall frequency and flux after fixing CSA. Additionally, the rainfall frequency and flux decrease almost linearly with fine aerosol, and are gradually stabilized after 2 μg m^{-3} (Fig. 3b, c). After fixing fine aerosol, a much stronger enhancement effect of CSA on warm rainfall properties (Fig. 3d, f) is revealed with respect to the general results mixed with fine aerosol (Fig. 2d, f). Similarly, the r_e continuously rises with the increasing CSA with an average increment of 8.3 ± 1.1 μm compared to 0.9 ± 0.6 μm without the fixed fine aerosols (Fig. 2d).

To account for meteorological variability that controls mainly the vertical development of clouds, the results in Fig. 3 are further divided into 3 bins of fixed LWP and plotted as Figs. 4 and 5. For fixed LWP and CSA, increasing fine aerosol from lowest to highest concentration bin (0.48 μg m^{-3} to 6.59 μg m^{-3}) decreases rainfall flux by an averaged factor of 1/4 (i.e., 0.26 ± 0.13; Fig. 4 and Table S1). In contrast, for fixed LWP and fine aerosol, increasing CSA from lowest to highest concentration bin (8.23 μg m^{-3} to 75.46 μg m^{-3}) increases rainfall flux by an averaged factor of 4 (i.e., 4.02 ± 2.15; Fig. 5 and Table S2). The effects on r_e were consistent with the effect on rainfall. The effects on both r_e and rainfall were larger for higher LWP as deeper clouds can provide a greater range for aerosol-driven warm rain variations.

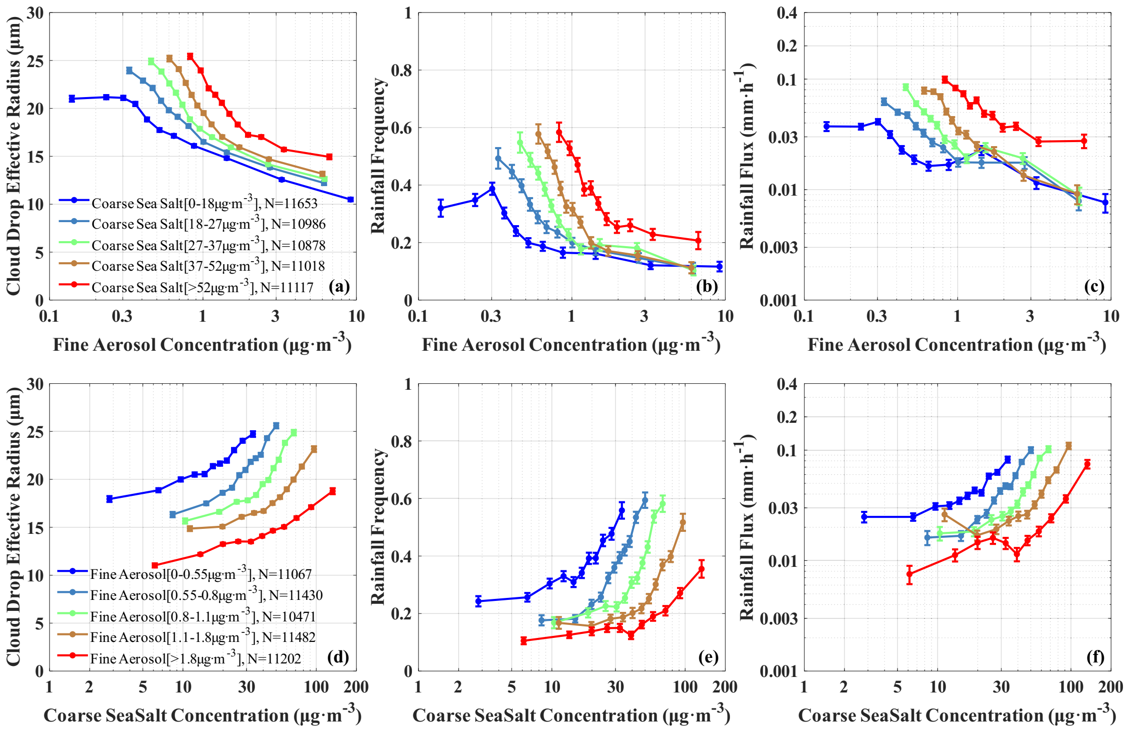

Fig. 3 Aerosol-driven cloud drop effective radius (r_e) and rainfall variations for fine aerosol (top) and coarse sea spray aerosols (CSA) (bottom) concentrations at the constant bins of another aerosol type. Shown are **a** r_e, **b** rainfall frequency, and **c** rainfall flux (including both rainfall and non-rainfall cases) driven by fine aerosol. The **d–f** are the same as **a–c**, but for CSA. The quantiles of the average for the 11 aerosol bins and vertical error bars are the same as in Fig. 2.

Further, we stratified the analyses by correlated meteorological parameters to disentangle aerosol-cloud effects from meteorological variability (Fig. S3). The parameters include temperature (850 hPa), specific humidity (850 hPa), vertical velocity (850 hPa), sea surface temperature, lower troposphere stability, convective available potential energy (CAPE), and surface wind speed. These results indicate that the rain suppression effect of fine aerosol (Fig. S4–S10) and the comparable rain enhancement effect of CSA (S11–S17) are independent of the meteorological conditions. Especially, since CSA is highly and positively correlated with surface wind speed ($R = 0.72$), we stratified the effect of sea spray by surface wind speed to separate the effects of wind and CSA (Fig. S11).

When surface wind speed is fixed, the susceptibility (i.e., d(r_e)/dln(CSA concentration)) of cloud and precipitation properties to CSA is larger than the results without the fixed wind speed (Fig. 3d, f), and becomes stronger with the increase in wind speed. The average susceptibility of r_e, rainfall frequency, and flux to CSA concentration are 3.80 ± 1.27, 0.16 ± 0.07, and 0.030 ± 0.012, respectively, when the surface wind speed is not fixed (Fig. 3d, f). However, the strongest susceptibilities of r_e, rainfall frequency, and flux occur under the highest surface wind speed condition with average susceptibility of 5.53 ± 1.90, 0.31 ± 0.11, and 0.066 ± 0.022, respectively. It may be attributed to the greater vertical transportation of CSA during stronger surface wind speed, thus facilitating a more effective interaction of CSA to warm clouds.

The effects of fine aerosol and CSA on r_e, rainfall frequency, and flux offset each other on statistical average, but not for individual realizations. Additionally, these large and contrasting effects are independent on meteorological conditions. These demonstrate that influence of GCCN cannot be ignored when analyzing the influence of fine aerosols on warm clouds. CSA can effectively weaken the precipitation inhibition caused by fine aerosol. Our findings suggest that the effect of CCN on warm precipitation was underestimated in previous studies because the effect of GCCN was not considered[9,10,21].

Parameterization of warm rain variations driven by two aerosol types. Inaccurate and incomprehensive parameterization of aerosol-cloud interactions largely contributes to the uncertainty of the climate models. To provide a reference for a parameterization that may be applicable in precipitation and climate models, multiple regression is used to quantify the sensitivity of warm rain to both fine and CSA aerosols. The multiple regression for cloud or rainfall properties was calculated as a quadratic non-linear function of fine aerosol, CSA, and LWP. The detailed method for multiple regression is provided in Methods. The results show that the observed r_e, rainfall frequency, and rainfall flux are highly correlated with the predicted results based on the multiple non-linear equations ($R^2 = 0.95$, 0.93, and 0.92). The coefficients of the regression equations are given in Table S3.

Figure 6 shows the predicted r_e, rainfall frequency, and flux at fixed low, moderate and high LWP based on the multiple non-linear regression model. The results show that the warm rain is simultaneously suppressed by fine aerosol but enhanced by CSA. For the same fixed LWP, r_e, rain frequency and flux consistently reach to the maximum under low fine aerosol and high CSA conditions. Conversely, the minimum occurs under high fine aerosol and low CSA conditions. Additionally, with the increment of LWP, clouds become thicker, and r_e and rainfall are simultaneously enhanced. In general, the cloud properties predicted by the multiple regression are in good agreement with the observations (Figs. 4 and 5). Figure S18 shows the full distribution of the cases, including the rare situations of high fine aerosol but low CSA loadings, and low fine aerosol but high CSA loadings. The extrapolation of the regression model at unpopulated areas in the parameter space leads to some inconsistencies

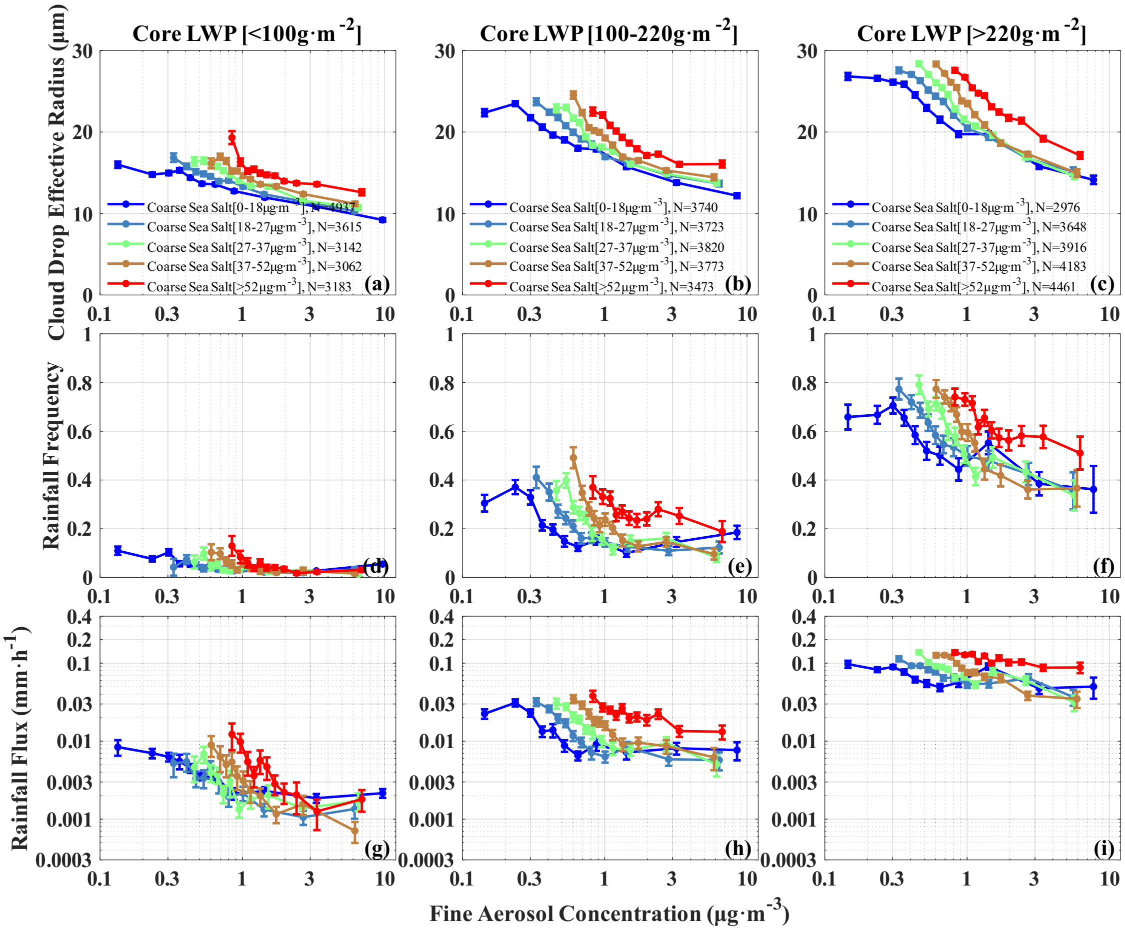

Fig. 4 Aerosol-driven cloud drop effective radius (r_e) and rainfall variations of warm clouds for fine aerosol concentration under different constant intervals of coarse sea spray aerosols (CSA) concentration and cloud liquid water path (LWP). The three columns represent low, moderate, and high cloud liquid water path, respectively. Shown are r_e (**a–c**), rainfall frequency (**d–f**), and **g–i** rainfall flux (including both rainfall and non-rainfall cases). The color lines connect the dots, which are the averaged r_e, rainfall frequency and flux at eleven bins of fine aerosol concentrations, including the 0–5%, 5–15%, 15–25%, 25–35%, 35–45%, 45–55%, 55–65%, 65–75%, 75–85%, 85–95%, and 95–100% quantiles. Vertical error bars indicate the standard error.

with the few actual cases there, as shown in the bottom-right and top-left corners of each panel of Fig. 6.

Discussion

Many previous studies that evaluated the effects of aerosols on precipitation did not consider the mixed effects of fine aerosol and CSA[9,10,21]. The simulations of Dziekan et al.[35] showed that the strongest contribution of GCCN to precipitation occurs when the CCN concentration is at low and moderate levels. Similar finding to the above-mentioned model study is observed in our study. Figure 3e shows the enhancement of rainfall frequency caused by CSA is stronger (enhanced by up to 0.4) when the fine aerosol concentration is low or moderate, and this enhancement becomes weaker under the heavy fine aerosol condition, even decreased to 0.1 when fine aerosol concentration is beyond 3 $\mu g\,m^{-3}$ (Fig. 3b). At high fine aerosol concentration, the droplets formed by CCN are extremely small, and they are difficult to be collected effectively by the large cloud droplets formed on the GCCN[35].

Our results demonstrate that the effects of fine aerosol and CSA on marine warm rain are opposite, comparable and independent, and they tend to offset each other when both aerosol types co-exist. The coexistence of fine aerosol and CSA leads to the observed sensitivities of warm rainfall to aerosols being falsely weak. Especially over ocean, the observed regulation of fine aerosols on warm rain is underestimated due to the co-existing abundant CSA. Therefore, the effects of fine aerosol and CSA should be studied comprehensively and independently.

Since the start of the industrial era, the emission of anthropogenic aerosols has grown dramatically, including sulfate aerosol, black carbon, and organic carbon[38]. To mitigate aerosol pollution, governments worldwide are taking actions to reduce anthropogenic aerosol emissions[38]. In response, most of the projections indicate an obvious reduction in future anthropogenic aerosols (the main parts of CCN). The sea salt, as a natural aerosol type, is mainly influenced by sea surface wind and sea surface temperature[39], may not change a great deal in the short term, but the change with global warming remains uncertain. Gettelman et al.[40] indicate that sea salt has a strong effect on cloud feedbacks in future climate with the increasing wind speed based on model prediction, mainly over the Southern Oceans. While they suggested a negative radiative feedback due to sea salt increasing cloud drop concentrations, the present study shows that the added sea spray increases substantially the r_e and hence reduces respectively the cloud drop concentrations. This is expected to incur a positive cloud feedback and thus contribute to the climatic warming. Therefore, with possible less CCN and uncertain CSA in the future, warm rainfall will probably occur more frequently.

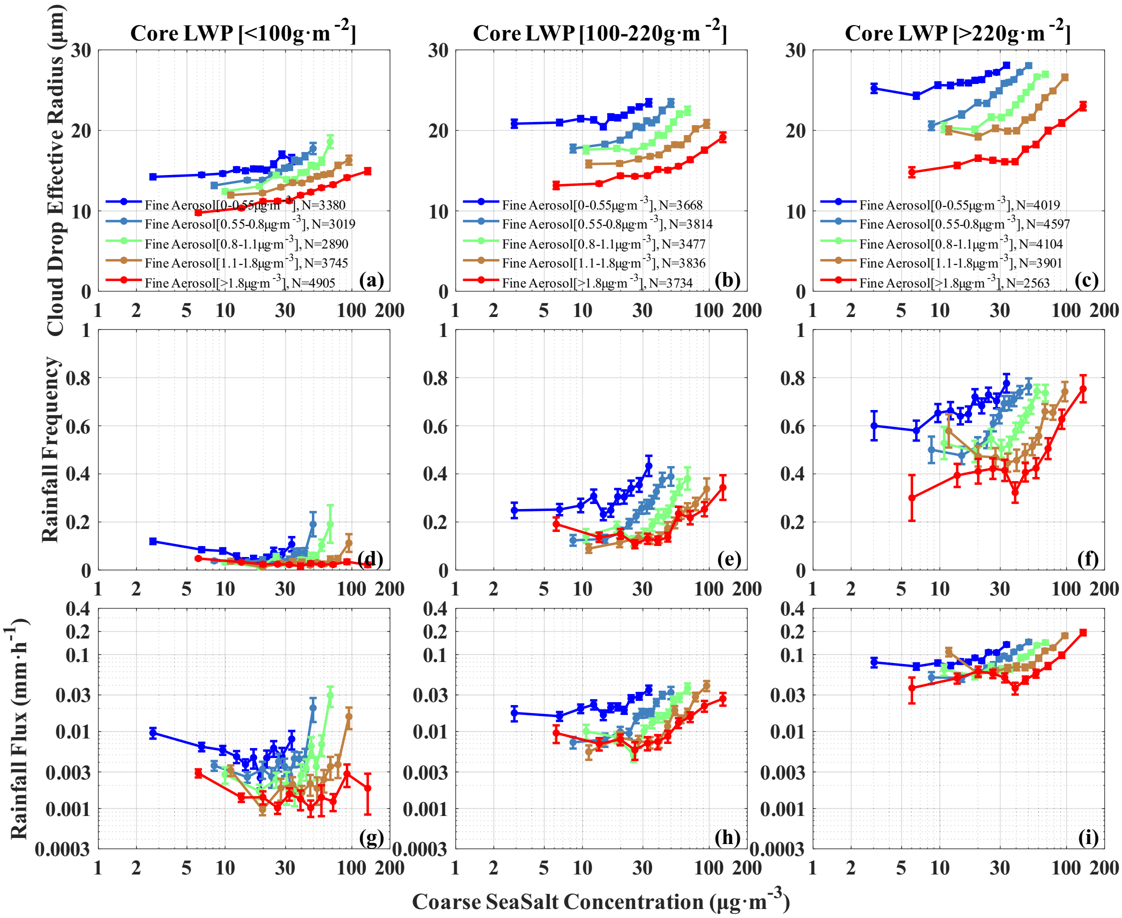

Fig. 5 Aerosol-driven cloud drop effective radius (r_e) and rainfall variations of warm clouds for coarse sea spray aerosols (CSA) concentration under different constant intervals of fine aerosol concentration and cloud liquid water path (LWP). The three columns represent low, moderate, and high cloud liquid water path, respectively. Shown are r_e (**a–c**), rainfall frequency (**d–f**), and **g–i** rainfall flux (including both rainfall and non-rainfall cases). The color lines connect the dots, which are the averaged r_e, rainfall frequency and flux at eleven bins of CSA concentrations, including the 0–5%, 5–15%, 15–25%, 25–35%, 35–45%, 45–55%, 55–65%, 65–75%, 75–85%, 85–95%, and 95–100% quantiles. Vertical error bars indicate the standard error.

This study quantifies the effects of CCN and GCCN on warm rainfall after isolating meteorological influence. The main conclusions are illustrated in Fig. 7 as follows.

(a) LWP dominates the formation and occurrence of warm rain (Figs. 1 and S3). Fixing LWP to isolate the effect of aerosols shows only a moderate fine aerosol effect suppressing rain by an average factor of 0.56 ± 0.32 (Fig. 2) when adding fine aerosols from the lowest to the highest observed concentrations. Adding CSA shows only a very small rain enhancement.

(b) When isolating the fine and coarse aerosol effects, both become much larger and comparable in magnitude but with opposite signs (Fig. 3). When fixing coarse aerosols and LWP, fine aerosol strongly suppresses rainfall flux by an average factor of 1/4. The r_e decreases by an average of −9.2 μm, or −40% (Table S1 and Fig. 4). Conversely, when fixing both LWP and fine aerosol, CSA strongly enhances rainfall flux by an average factor of 4. The r_e increases by an average of 5.3 μm, or 35% (Table S2 and Fig. 5).

(c) Thicker clouds (larger LWP) have a larger response to aerosols (Figs. 4 and 5). Fine aerosol decreases r_e and rainfall frequency by an average of −6.1 μm and −7% for shallow clouds (LWP < 100 g m^{-2}), while the related suppression reach −12.2 μm and −37% for thick clouds (LWP > 220 g m^{-2}). Additionally, the comparable effects to warm rain are also observed from CSA but with opposite signs.

(d) The effects of fine aerosol and CSA on warm rain are opposite and comparable in magnitude, and they are independent on meteorological conditions (Figs. S4–S17). Moreover, at stronger surface wind speed the effect of coarse aerosols on rain enhancement is larger, probably because a stronger wind can transport CSA to higher altitudes, thus facilitating a stronger interaction of CSA with warm clouds (Fig. S11).

Isolating the large contrasting effects of fine and coarse aerosols shows that much of their effects are often (but not always) masked when they are averaged together. This explains why these large effects have been underappreciated until now. Moreover, abundant CSA over ocean increases the warm rain supports the hypothesis that aerosol differences can explain some of the land-ocean warm rain contrast. Additionally, the influence of CCN and GCCN should be fully and independently considered in climate models when quantifying the precipitation and the indirect effects of aerosols. The quantitative information given by our methods can be used as a reference for the parameterization of warm rainfall processes by CCN and GCCN. A full consideration of the combined effect of fine aerosol and CSA in global climate models is essential for improving future climate projections.

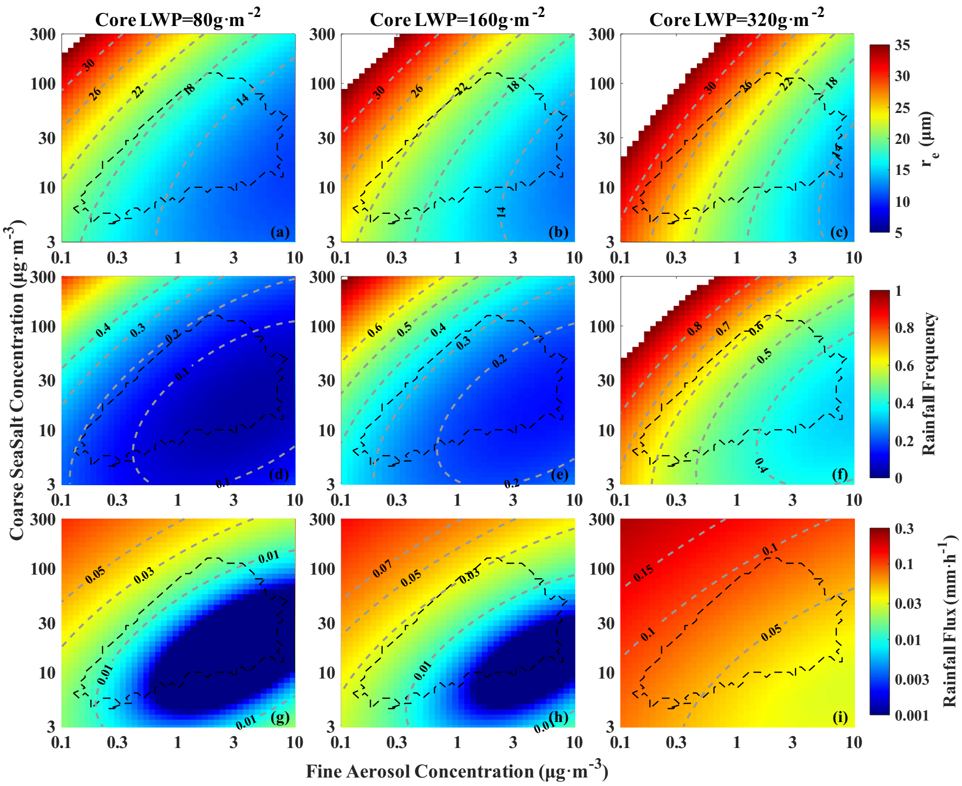

Fig. 6 Parameterization of warm rain variations driven by fine aerosol and coarse sea spray aerosols (CSA) at fixed cloud liquid water path (LWP) based on the multiple non-linear regression model. The three rows indicate the predicted aerosol-driven variations of r_e (**a–c**), rainfall frequency (**d–f**), and rainfall flux (**g–i**) under different constant LWP conditions. The three columns represent the low, moderate, and high LWP conditions, which are equal to 80, 160, and 320 g m^{-2}, respectively. The gray dotted lines represent the contours of cloud or rainfall properties. The black dashed line indicates the distribution of the aerosols, with the sample size of each fine aerosol and CSA bins above 10, as same as the black dashed line in Fig. S18a.

Methods

Data sources. Warm rain considerably influences tropical oceans and accounts for nearly 100% of rainfall occurrence over large areas[41]. The focus of this research is the oceanic region from −50° W to 50° E and −30° S to 30° N. The study period covers March 2014 (start time of precipitation data) to December 2017. As shown in Table S4, the cloud and aerosol parameters were obtained from the METEOSAT Second Generation (MSG) geostationary satellite and Modern-Era Retrospective Analysis for Research and Application Version 2 (MERRA-2) reanalysis data, respectively. The precipitation parameters were obtained from the Global Precipitation Measurement (GPM) Dual-frequency Precipitation Radar (DPR) dataset. The MERRA-2 reanalysis data does not provide the convective available potential energy (CAPE), which indicates the potential energy for cloud vertical development. To make the source of meteorological data consistent, we got the meteorological condition of water clouds based on the National Centers for Environmental Prediction (NCEP) reanalysis data.

MERRA-2 aerosol data have five aerosol species: dust, sea salt, sulfates, organic carbon, and black carbon[42]. The long-term observed aerosol optical depths (AOD) are assimilated in MERRA-2, such as Moderate Resolution Imaging Spectroradiometer and Aerosol Robotic Network (AERONET)[39]. The speciation, size, and vertical distribution of the aerosol are constrained by the Goddard Earth Observing System Data Assimilation System version 5 earth system model. Additionally, sea salt and dust aerosols in MERRA-2 are mainly dependent on assimilated surface wind speed[43]. The other aerosol types (black carbon, organic carbon, and sulfate) are mainly prescribed from updated emissions inventories of both natural and anthropogenic sources[43]. Previous studies have validated the reliability of MERRA-2 aerosol data[43,44]. Based on the globally long-term comparison, the MERRA-2 and AERONET AOD have a good agreement with an average correlation of 0.84, and it even reaches 0.93 over ocean[39,43,44].

All data were initially matched at the spatial resolution of MSG Geostationary Earth Radiation Budget (GERB; 9 × 9 km) to evaluate aerosol-driven radiative forcing from oceanic warm clouds in future studies. MERRA-2 aerosol and NCEP meteorology data were matched at a fixed time interval of the MSG CLoud property dAtAset by using the SEVIRI product (CLAAS) based on linear interpolation in time. The GPM DPR instantaneous observation was matched with the interpolated aerosol, cloud, and meteorology data within a ± 15 min timespan of MSG observation time. The details are presented in Fig. S19.

Data selection and properties. All data were eventually averaged into 1° × 1° grids as samples (Fig. S19). As this study focused on oceanic warm clouds, the samples with only liquid-phase clouds and cloud top temperature (CTT) >265 K were selected. Also, the satellite cloud retrieval error caused by the large solar zenith angle was avoided by selecting data between 8 and 16 o'clock local time. Additionally, surface clutter always prevents radar from observing near-surface precipitation, causing a large bias of rainfall rate observed by GPM DPR at near-surface altitude[45]. Here, the samples were rejected when cloud top heights at the convective core area of the water cloud were less than 1.2 km, as physically rain mainly occurs in the convective core area. The core area is defined as the water cloud pixels with the highest 10% in cloud optical depth at a 1° × 1° grid, referring to the study of Zhu et al.[46].

The cloud parameters r_e and LWP from MSG CLAAS data represent the effective radius of cloud droplets and the total amount of liquid water from cloud base to cloud top, respectively. Referring to the study of Zhu et al.[46], the averaged r_e and LWP over the convective core area within a 1° × 1° scene (highest 10% of cloud optical depth) are used as the representative of cloud properties of the 1° × 1° samples. The cloud at the convective core area is almost adiabatic, which is relatively less influenced by the external environment compared to the cloud edge[3]. Physically, rain should mainly occur in the convective core area. Therefore, the samples that rain is detected by GPM DPR at their core area are identified as rain samples. Here, rainfall frequency refers to the proportion of rain samples to all available samples. Rainfall flux equals the integrated rainfall rate from rain pixels divided by the number of total pixels in the fixed 1° × 1° grid with the unit of mm h^{-1}.

Fine aerosol indicates the sum mass of aerosols with a radius below 1 μm, including sulfates, organic carbon, black carbon, and fine sea salt, which is used as the proxy of CCN. CSA indicates the mass of sea salt with a radius above 1 μm, which is used as the proxy of GCCN. The aerosol mass concentrations are obtained at the surface level. Finally, we obtained 55652 available 1° × 1° samples that meet all the conditions mentioned above. Their spatial distribution is shown in Fig. S20. The samples included 16,443 rain samples and 39,209 non-rain samples.

Multiple regression for parameterization of aerosol-driven warm rain variations. Appropriate parameterization of aerosol-cloud interactions is key to the accurate simulation of the climate model. Here, we use the multiple

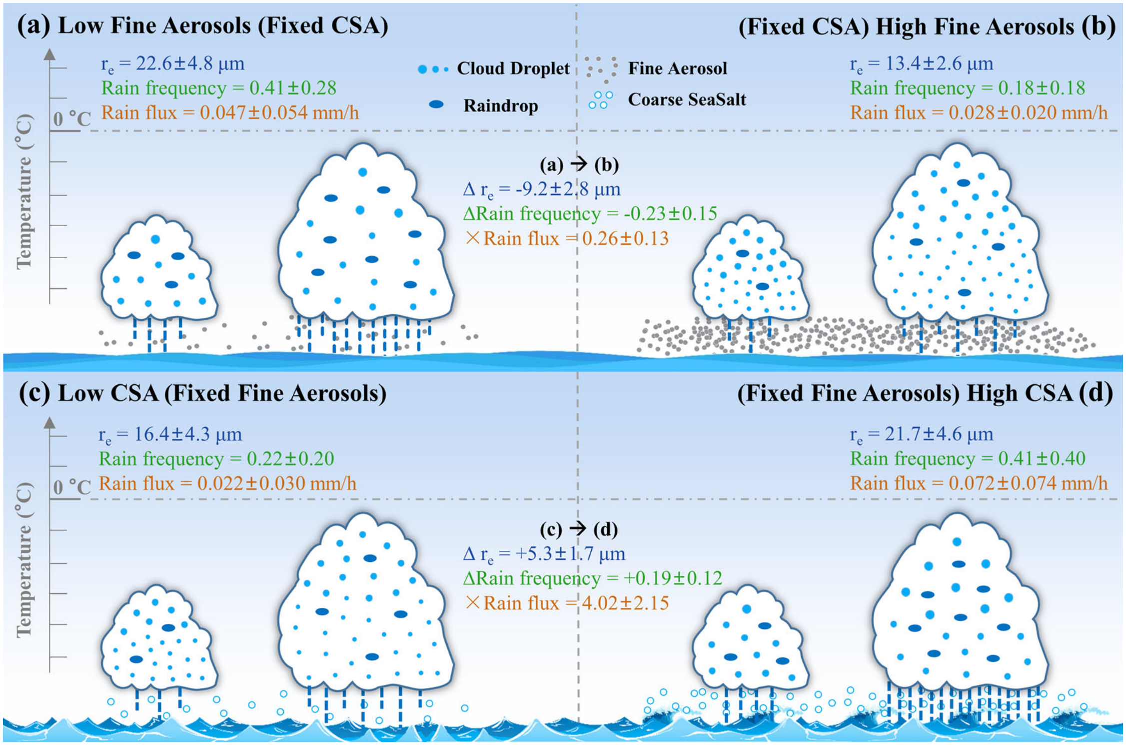

Fig. 7 Conceptual representation of the comparable but opposite effects of fine aerosol and coarse sea spray aerosols (CSA) on the rainfall of marine warm clouds. The averaged r_e and rainfall of shallow (low LWP) and thick (high LWP) warm clouds are characterized at different fine aerosol and CSA conditions, including (**a**, **b**) low and high fine aerosol concentrations at fixed both LWP and CSA concentrations, **c**, **d** low and high CSA concentrations at fixed both of LWP and fine aerosol concentrations. The changes upon transition between states are marked by the arrows and the adjacent numbers. With the added fine aerosols from low to high concentration (from **a** to **b**), the r_e, rainfall frequency, and flux are synchronously reduced by added drop concentrations whatever the low and high CSA concentrations. In contrast, the added CSA from low to high concentration (from **c** to **d**) activates the early formation of large cloud drops and suppresses the activation of fine aerosols, thus simultaneously increases r_e, rainfall frequency and rainfall flux. Statistics of averaged r_e and rainfall of panels **a**, **b** were obtained from Fig. 4 and Table S1, while panels **c**, **d** were from Fig. 5 and Table S2.

regression method to parameterize the sensitivity of warm rain on both fine and CSA aerosols. Multiple regression is a robust method to capture the statistical relationship among multiple independent variables based on the non-linear fitting, and has been widely used in aerosol-cloud interaction studies[3,6]. The main steps are summarized as follows:

(1) To isolate the interactions between fine aerosol and CSA, the r_e of all cases are separately divided into different independent fine aerosol and CSA bins. The specific 9 bins of fine aerosol and CSA concentrations are 0–5%, 5–10%, 10–20%, 20–40%, 40–60%, 60–80%, 80–90%, 90–95%, and 95–100% quantiles, respectively. To ensure the effective sampling of the data observation range, we use the finer bin at high and low concentrations of fine aerosol and CSA.
(2) Further, all cases are also divided into five LWP bins with equal sample size to constrain the meteorological influence, including 0–20%, 20–40%, 40–60%, 60–80%, and 80–100% quantiles. Theoretically, we get 405 independent bins. To remove spurious results, only the bins with sample sizes above 10 are incorporated into the regression.
(3) The bin-averaged r_e is fitted as the function of fine aerosol, CSA, and LWP based on multi-variates second-order fitting referring to the previous study[3]. The coefficients and fitted regression equation are provided in Table S3. The same processes are repeated for rainfall frequency and flux.

Data availability

Cloud data is obtained from MSG CLAAS (https://wui.cmsaf.eu/safira) provided by EUMETSAT Satellite Application Facility on Climate Monitoring. Precipitation data is obtained from GPM 2ADPR product (https://storm.pps.eosdis.nasa.gov/storm) provided by NASA/Goddard Space Flight Center's science team. Meteorology data is obtained from NCEP FNL product (https://rda.ucar.edu/datasets/ds083.2) provided by National Center for Atmospheric. Aerosol data is obtained from MERRA-2 reanalysis datasets (https://gmao.gsfc.nasa.gov/reanalysis/MERRA-2) provided by the NASA Global Modeling and Assimilation Office. The dataset containing all the relevant properties of the main figures is in Supplementary Data.

Code availability

The computer codes used to analyze the data are available from the corresponding author on request.

Received: 17 May 2022; Accepted: 22 September 2022;
Published online: 07 October 2022

References

1. Hartmann, D. L. & Short, D. A. On the use of earth radiation budget statistics for studies of clouds and climate. *J. Atmos. Sci.* **37**, 1233–1250 (1980).
2. Slingo. Sensitivity of the Earth's radiation budget to changes in low clouds. *Nature* **343**, 49–51 (1990).
3. Rosenfeld, D. et al. Aerosol-driven droplet concentrations dominate coverage and water of oceanic low-level clouds. *Science* https://doi.org/10.1126/science.aav0566 (2019).
4. Twomey, S. The influence of pollution on the shortwave albedo of clouds. *J. Atmos. Sci.* **34**, 1149–1152 (1977).
5. Albrecht, B. A. Aerosols, cloud microphysics, and fractional cloudiness. *Science* **245**, 1227–1230 (1989).
6. Li, Z. et al. Long-term impacts of aerosols on the vertical development of clouds and precipitation. *Nat. Geosci.* **4**, 888–894 (2011).
7. Wang, S., Wang, Q. & Feingold, G. Turbulence, condensation, and liquid water transport in numerically simulated nonprecipitating stratocumulus clouds. *J. Atmos. Sci.* **60**, 262–278 (2003).

8. Chen, Y.-C., Christensen, M. W., Stephens, G. L. & Seinfeld, J. H. Satellite-based estimate of global aerosol–cloud radiative forcing by marine warm clouds. *Nat. Geosci.* **7**, 643–646 (2014).
9. Christensen, M. W. & Stephens, G. L. Microphysical and macrophysical responses of marine stratocumulus polluted by underlying ships: 2. Impacts of haze on precipitating clouds. *J. Geophys. Res.: Atmos.* https://doi.org/10.1029/2011jd017125 (2012).
10. Fan, C. et al. Strong precipitation suppression by aerosols in marine low clouds. *Geophys. Res. Lett.* https://doi.org/10.1029/2019gl086207 (2020).
11. Koren, I., Dagan, G. & Altaratz, O. From aerosol-limited to invigoration of warm convective clouds. *Science* **344**, 1143–1146 (2014).
12. Dagan, G., Koren, I. & Altaratz, O. Aerosol effects on the timing of warm rain processes. *Geophys. Res. Lett.* **42**, 4590–4598 (2015).
13. Zhu, Y., Rosenfeld, D., Yu, X. & Li, Z. Separating aerosol microphysical effects and satellite measurement artifacts of the relationships between warm rain onset height and aerosol optical depth. *J. Geophys. Res.: Atmos.* **120**, 7726–7736 (2015).
14. Braga, R. C. et al. Further evidence for CCN aerosol concentrations determining the height of warm rain and ice initiation in convective clouds over the Amazon basin. *Atmos. Chem. Phys.* **17**, 14433–14456 (2017).
15. Fossum, K. N. et al. Sea-spray regulates sulfate cloud droplet activation over oceans. *Npj Clim. Atmos. Sci.* **3**, 1–6 (2020).
16. Pan, Z. et al. Coarse sea spray inhibits lightning. *Nat. Commun.* **13**, 1–7 (2022).
17. Feingold, G., Cotton, W. R., Kreidenweis, S. M. & Davis, J. T. The impact of giant cloud condensation nuclei on drizzle formation in stratocumulus: Implications for cloud radiative properties. *J. Atmos. Sci.* **56**, 4100–4117 (1999).
18. Posselt, R. & Lohmann, U. Influence of giant CCN on warm rain processes in the ECHAM5 GCM. *Atmos. Chem. Phys.* **8**, 3769–3788 (2008).
19. Yin, Y., Levin, Z., Reisin, T. G. & Tzivion, S. The effects of giant cloud condensation nuclei on the development of precipitation in convective clouds —a numerical study. *Atmos. Res.* **53**, 91–116 (2000).
20. Rosenfeld, D. et al. The Role of Sea Spray in Cleansing Air Pollution over Ocean via Cloud Processes. *Science* **297**, 1667–1670 (2002).
21. L'Ecuyer, T. S., Berg, W., Haynes, J., Lebsock, M. & Takemura, T. Global observations of aerosol impacts on precipitation occurrence in warm maritime clouds. *J. Geophys. Res.* https://doi.org/10.1029/2008jd011273 (2009).
22. Dror, T. et al. Sensitivity of warm clouds to large particles in measured marine aerosol size distributions – a theoretical study. *Atmos. Chem. Phys.* **20**, 15297–15306 (2020).
23. Blyth, A. M. et al. The production of warm rain in shallow maritime cumulus clouds. *Quart. J. R. Meteorol. Soc.* **139**, 20–31 (2013).
24. Lehahn, Y., Koren, I., Altaratz, O. & Kostinski, A. B. Effect of coarse marine aerosols on stratocumulus clouds. *Geophys. Res. Lett.* https://doi.org/10.1029/2011GL048504 (2011).
25. Rosenfeld, D., Axisa, D., Woodley, W. L. & Lahav, R. A quest for effective hygroscopic cloud seeding. *J. Appl. Meteorol. Climatol.* **49**, 1548–1562 (2010).
26. Lohmann, U., Koren, I. & Kaufman, Y. J. Disentangling the role of microphysical and dynamical effects in determining cloud properties over the Atlantic. *J. Geophys. Res. Lett.* https://doi.org/10.1029/2005GL024625 (2006).
27. Mauger, G. S. & Norris, J. R. Meteorological bias in satellite estimates of aerosol-cloud relationships. *Geophys. Res. Lett.* https://doi.org/10.1029/2007gl029952 (2007).
28. Christensen, M. W. et al. Opportunistic experiments to constrain aerosol effective radiative forcing. *Atmos. Chem. Phys.* **22**, 641–674 (2022).
29. Yang, Y. et al. Rain-aerosol relationships influenced by wind speed. *Geophys. Res. Lett.* **43**, 2267–2274 (2016).
30. Mülmenstädt, J., Sourdeval, O., Delanoë, J. & Quaas, J. Frequency of occurrence of rain from liquid-, mixed-, and ice-phase clouds derived from A-Train satellite retrievals. *Geophys. Res. Lett.* **42**, 6502–6509 (2015).
31. Williams, E. & Stanfill, S. The physical origin of the land–ocean contrast in lightning activity. *C. R. Phys.* **3**, 1277–1292 (2002).
32. Takahashi, H., Suzuki, K. & Stephens, G. Land–ocean differences in the warm-rain formation process in satellite and ground-based observations and model simulations. *Quart. J. R. Meteorol. Soc.* **143**, 1804–1815 (2017).
33. Jorgensen, D. P. & LeMone, M. A. Vertical velocity characteristics of oceanic convection. *J. Atmos. Sci.* **46**, 621–640 (1989).
34. Wood, R., Hartmann, D. L. & Kubar, T. L. Understanding the importance of microphysics and macrophysics for warm rain in marine low clouds. Part I: satellite observations. *J. Atmos. Sci.* **66**, 2953–2972 (2009).
35. Dziekan, P., Jensen, J. B., Grabowski, W. W. & Pawlowska, H. Impact of giant sea salt aerosol particles on precipitation in marine cumuli and stratocumuli: lagrangian cloud model simulations. *J. Atmos. Sci.* https://doi.org/10.1175/jas-d-21-0041.1 (2021).
36. Rosenfeld, D. et al. Global observations of aerosol-cloud-precipitation-climate interactions. *Rev. Geophys.* **52**, 750–808 (2014).
37. Pan, Z. et al. Observational quantification of aerosol invigoration for deep convective cloud lifecycle properties based on geostationary satellite. *J. Geophys. Res.: Atmos.* https://doi.org/10.1029/2020jd034275 (2021).
38. Levy, H. et al. The roles of aerosol direct and indirect effects in past and future climate change. *J. Geophys. Res. Atmos.* **118**, 4521–4532 (2013).
39. Randles, C. et al. The MERRA-2 aerosol reanalysis, 1980 onward. Part I: System description and data assimilation evaluation. *J. Clim.* **30**, 6823–6850 (2017).
40. Gettelman, A., Lin, L., Medeiros, B. & Olson, J. Climate feedback variance and the interaction of aerosol forcing and feedbacks. *J. Clim.* **29**, 6659–6675 (2016).
41. Nelson, E. L. & L'Ecuyer, T. S. Global character of latent heat release in oceanic warm rain systems. *J. Geophys. Res. Atmos.* **123**, 4797–4817 (2018).
42. Gelaro, R. et al. The modern-era retrospective analysis for research and applications, version 2 (MERRA-2). *J. Clim.* **30**, 5419–5454 (2017).
43. Buchard, V. et al. Using the OMI aerosol index and absorption aerosol optical depth to evaluate the NASA MERRA Aerosol Reanalysis. *Atmos. Chem. Phys.* **15**, 5743–5760 (2015).
44. Bian, H. et al. Observationally constrained analysis of sea salt aerosol in the marine atmosphere. *Atmos. Chem. Phys.* **19**, 10773–10785 (2019).
45. Kubota, T. et al. A statistical method for reducing sidelobe clutter for the Ku-band precipitation radar on board the GPM core observatory. *J. Atmos. Ocean. Technol.* **33**, 1413–1428 (2016).
46. Zhu, Y., Rosenfeld, D. & Li, Z. Under what conditions can we trust retrieved cloud drop concentrations in broken marine stratocumulus? *J. Geophys. Res.: Atmos.* **123**, 8754–8767 (2018).

Acknowledgements

This study is partially supported by The Reef Restoration and Adaptation Program aims to develop effective interventions to help the Reef resist, adapt to, and recover from the impacts of climate change. In addition, it was supported by the National Natural Science Foundation of China (41971285 and 41627804) and Wuhan University Specific Fund for Major School-level Internationalization Initiatives. Numerical calculations in this paper are performed on the supercomputing system in the Supercomputing Center of Wuhan University.

Author contributions

D.R. and Z.P. designed this study; F.L., Z.P., and F.M. acquired and processed the data; F.L., Z.P., D.R., F.M., and L.Z. carried out analyses and interpreted data; F.L, Z.P., D.R., and F.M. wrote the manuscript; L.Z., Y.Z., J.Y., and W.G. contributed to the comparisons with other studies and discussion. All co-authors commented on and reviewed the manuscript.

Competing interests

The authors declare no competing interests.

Additional information

Supplementary information The online version contains supplementary material available at https://doi.org/10.1038/s43247-022-00562-y.

Correspondence and requests for materials should be addressed to Zengxin Pan.

Peer review information *Communications Earth & Environment* thanks Michael Diamond and the other, anonymous, reviewer(s) for their contribution to the peer review of this work. Primary Handling Editors: Kerstin Schepanski and Clare Davis.